Estuarine, Coastal and Shelf Science 219 (2019) 372–383

Contents lists available at ScienceDirect

Estuarine, Coastal and Shelf Science

journal homepage: www.elsevier.com/locate/ecss

Hydrological and biogeochemical controls on Fe cycling at the Krabbenkreek supratidal/intertidal zone, the Netherlands: Why does the Fe pump sputter?

Alejandra Morera-Chavarría[a,*], Jasper Griffioen[b,c], Isabel Chueca-García[b], Marta Faneca-Sánchez[d], Thilo Behrends[a]

[a] Faculty of Geosciences, Department of Earth Sciences – Geochemistry, Utrecht University, P.O. Box 80 021, 3508TA, Utrecht, the Netherlands
[b] TNO Geological Survey of the Netherlands, P.O. Box 80 015, 3508 TA, Utrecht, the Netherlands
[c] Faculty of Geosciences, Copernicus Institute of Sustainable Development, Utrecht University, P.O. Box 80 115, 3508 TC, Utrecht, the Netherlands
[d] Deltares, P.O. Box 85 467, 3508 AL, Utrecht, the Netherlands

ARTICLE INFO

Keywords:
Estuarine sediments
Iron biogeochemistry
Hydrogeological model
Tidal flats

ABSTRACT

Frequent and unexplained iron enrichments have been localized in buried, Holocene, marine sediments in coastal areas. These buried sediments are nowadays often part of groundwater systems in densely populated deltas. Here, the Krabbenkreek intertidal/supratidal area in the Netherlands is considered as a present analogue for diagenetic processes in these near-shore sediments. We evaluate the role of tidally driven groundwater flow alternations on the transport and speciation of Fe in deep tidal sediments. This was achieved by examining geochemical sediment and porewater data in the context of 3-D geohydrological modelling results of the groundwater system. The Krabbenkreek area presents clear hydrologic and geochemical zonations across the supratidal/intertidal area. Due to the low hydraulic conductivity, groundwater flow and infiltration of rain water is limited in the mud-rich upper sediments of the supratidal flat. Despite tidal fluctuations of the hydraulic heads up to 1.5 m, the corresponding alternating groundwater flow is relatively minor in comparison to the net groundwater flow. Tidal variations in the groundwater force field alone did not lead to pronounced local enrichments in reactive Fe. Differences in reactive Fe contents in deep sediments can be related to textural differences, implying that no indications for local, diagenetic Fe enrichments were found in the sediments down to 5 m depth. Contents of FeS and amorphous Fe(III) are remarkably low indicating little current dynamics in Fe redox cycling in these deep sediments, while the porewater chemistry indicates that pyrite oxidation prevails. Long-term oxidation of pyrite is reflected by the presence of Fe(III) oxides in the high marsh sediments while pyrite still dominates in the middle marsh and the intertidal sediments. Absence of active Fe redox cycling can be attributed to low respiratory activity in the sediments. Previous studies reported that sedimentary organic matter in the vicinity of the investigated area can be predominately refractory, which can probably explain the low respiratory activity in the Krabbenkreek sediments.

1. Introduction

Tidal flats in coastal areas are highly dynamic zones subject to daily flood and ebb currents. These have an impact on physical and geochemical processes in both the sediment and the porewater. The sediments in these areas are typically redox stratified and the alternating flow can accentuate concentration profiles of redox sensitive elements at the transition from oxic to anoxic conditions (Froelich et al., 1979; Thullner et al., 2007). Some contaminants are redox sensitive elements and understanding the role of groundwater flow on their dynamics in estuarine settings can provide insight in the fate of these contaminants in rivers and estuaries (Zwolsman et al., 1993; Passos et al., 2010).

The impact of the tidal currents on the groundwater movement has been explored through both numerical simulations (e.g. Harvey et al., 1987; Gardner, 2005; Wilson and Gardner, 2006; Gibbes et al., 2008b; Xia and Li, 2012) and field measurements (e.g. Robinson et al., 1998; Hughes et al., 1998; Gibbes et al., 2008a; Røy et al., 2008; Xia and Li, 2012). These studies considered the groundwater flow in sandy tidal

* Corresponding author.
E-mail addresses: a.morerachavarria@uu.nl (A. Morera-Chavarría), j.griffioen@uu.nl (J. Griffioen), Isabel.Chueca@ciemat.es (I. Chueca-García), Marta.Faneca@deltares.nl (M. Faneca-Sánchez), t.behrends@uu.nl (T. Behrends).

https://doi.org/10.1016/j.ecss.2019.02.032
Received 20 March 2018; Received in revised form 4 February 2019; Accepted 11 February 2019
Available online 15 February 2019

flats and salt marsh soils at different scales that vary from cm to m. The aforementioned studies concluded that a variety of parameters play an important role determining the groundwater flow in tidally influenced areas. Such parameters include the geometry of the flats, extreme tidal events, salinity fluctuations, porosity and seasonal variations in rainfall. In the case of salt marshes, the composition of the top soil, its hydraulic properties, vegetation and evapotranspiration are also of importance in controlling the groundwater flow. The number of variables influencing the hydrodynamics of a particular tidal zone makes the groundwater flow patterns highly variable.

The biogeochemical cycles in these settings are often promoted by the large input of degradable organic matter (OM) (Lord and Church, 1983; Oenema, 1990a; Koch et al., 1992; Kostka et al., 2002; Pallud and van Cappellen, 2006; Gittel et al., 2008; Lemke et al., 2009). In these studies, the mineralisation of OM and nutrient cycling were investigated in the salt marsh soils (top 50 cm). The biogeochemical cycles of redox sensitive elements have been studied in both sediments (e.g. Suttill et al., 1982; Luther et al., 1982; Cutter and Velinsky, 1988; Baeyens et al., 1991; Kostka and Luther, 1994; Charette and Sholkovitz, 2002; Burton et al., 2006; Johnston et al., 2011; Kolditz et al., 2012) and porewater (e.g.; Burton et al., 2006; Beck et al., 2008a; Beck et al., 2008b; Morford et al., 2009; Beck et al., 2009; Kolditz et al., 2009; Kowalski et al., 2009; Beck & Brumsack, 2012). These studies also report intense Fe redox cycling in diverse tidal areas (e.g. Wadden Sea, Waquoit Bay, East Trinity) where the topography and the tides exert major controls on the redox zonations and related Fe speciation. As in tidal flats, oscillations in the hydrologic regime are the driving force in the development of concentration profiles of Fe in soils and aquifers. In gleysols, the zone of variable groundwater tables is indicated by pronounced local enrichments of Fe (oxy)(hydr)oxides (in the following collectively referred to as Fe oxides). Vertical movements of the redox boundary between reducing groundwater, containing dissolved ferrous iron (Fe(II)), and the oxygen containing unsaturated zone results in Fe (II) oxidation and Fe oxide precipitation in the affected soil horizon (Stoops and Eswaran, 1985; Appelo et al., 1999). Also, the formation of bog iron deposits in low relief areas near stream banks, small lakes and swamps is the consequence of Fe enrichments in the form of various Fe oxides including ferrihydrite and goethite (Stoops, 1983; Kaczorek and Sommer, 2003). These Fe oxides are the product of groundwater rich in dissolved Fe(II) flowing vertically and horizontally towards the aerated surfaces. Often, the oxidation of Fe is catalysed by bacteria (Crerar et al., 1979).

During the Holocene, surficial coastal sediments were buried in floodplains due to transgressive and regressive cycles, both in the Netherlands and elsewhere (Allen, 2000). These sediments are composed of estuarine, tidal and coastal deposits and features pronounced and unexplained pyrite enrichments (Vermooten et al., 2011; Griffioen et al., 2012). These buried floodplain sediments are nowadays often part of groundwater systems in densely populated deltas and the inventory of reactive minerals in the aquifers is of pivotal relevance for the groundwater quality. A representative of buried, coastal sediments from the Holocene is the Naaldwijk Formation in the Netherlands. This formation has elevated pyrite contents that reach up to 3% in sandy sediments and up to 6% in clay-rich ones (van Gaans et al., 2011; Griffioen et al., 2012). These contents are considerably higher than those found in soil profiles of Dutch supratidal flats, where contents usually vary around 1% with a maximum of 3% in clay-rich sediments (Oenema, 1988, 1990a).

The hydrology and Fe chemistry from the deep sediments from the Krabbenkreek intertidal/supratidal area were studied as present analogue for diagenetic processes in the near-shore sediments of the Naaldwijk Formation. We investigated the groundwater dynamics at the Krabbenkreek and geochemically characterized the deep sediments and porewater by focussing on processes controlling the transport and speciation of Fe. Here, the top soil (top 50 cm) from the Krabbenkreek was not geochemically characterized, as it was already extensively studied by Oenema (1988, 1990a,b), Oenema and DeLaune (1988), Ma et al. (2014), among others.

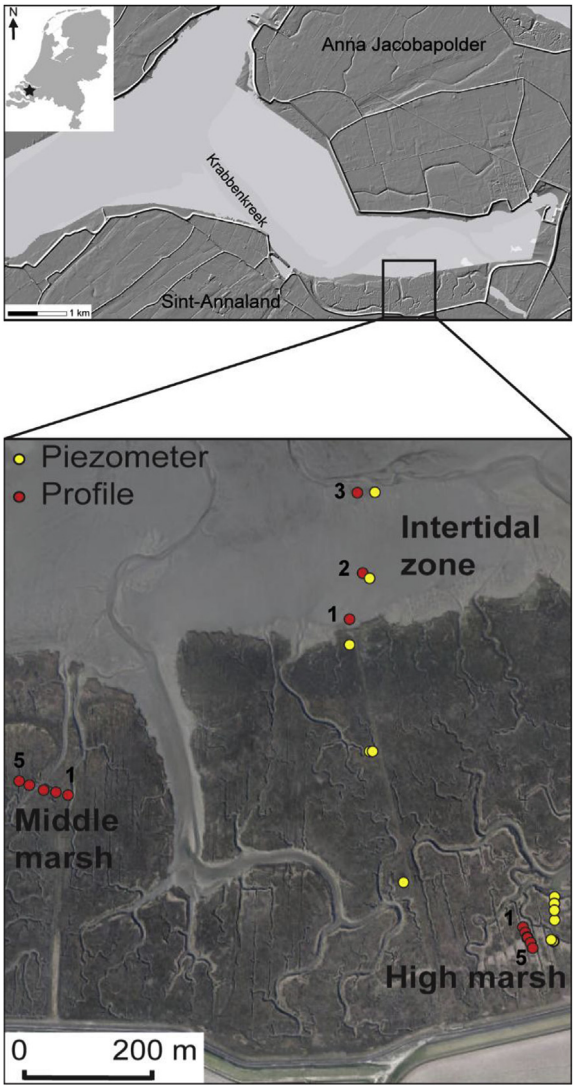

Fig. 1. Location of Krabbenkreek supratidal/intertidal area in the Eastern Scheldt, the Netherlands. Sampling transects and piezometer location in the supratidal zone (middle marsh and high marsh areas) and intertidal zones.

2. Materials and methods

2.1. Study area

The study site, Krabbenkreek, is located near the village of Sint Annaland, in the Eastern Scheldt estuary in the province of Zeeland, the Netherlands (Fig. 1). This region has a temperate maritime climate with a mean annual rainfall of c. 900 mm (Royal Netherlands Meteorological Institute (KNMI) a) and an annual potential evaporation of 500–650 mm (KNMI b). The Eastern Scheldt is limited by man-made dikes on three sides (Supplementary Fig. S1). After completing the construction of the Strom Surge Barrier and Compartment dams in 1986–1987 the tidal amplitude in the Scheldt estuary was reduced and some channels were abandoned (Oenema and DeLaune, 1988; Louters et al., 1998). The Krabbenkreek is located in a dead ending side arm of the Scheldt estuary. According to the Executive Agency of the Ministry of Infrastructure and Water Management of the Netherlands, this area presents a sinusoidal tide with average ~1.5 m amplitude and a 12 h period. Krabbenkreek is an area formed by intertidal and supratidal

flats. The supratidal flat comprises a marsh area (high marsh and middle marsh) which is part of a nature reserve (Fig. 1).

The vegetation at the Krabbenkreek area is dominated by *Halimione portulacoides, Festuca Rubra, Elytrigia atherica* (van Maldegem and de Jong, 2004). These vegetation types are characterized for having the majority of root mass within the top 30–40 cm below soil surface (Redelstein et al., 2018).

The coastal landscape of the southwestern Netherlands formed during the Holocene. The major driving forces for the coastal genesis in this area have been the rise in sea level, morphology during the early Holocene, availability and supply of sediments and human interference (Vos and van Heeringen, 1997; Vos et al., 2002). The construction of dikes contributed to the embankments of the adjacent polders (reclaimed lands) and formation of numerous marsh areas (Oenema and DeLaune, 1988; Ma et al., 2014) (Fig. S1).

The intertidal flats of the Eastern Scheldt are dynamic sedimentological areas, characterized by constant topographic changes. The tidal influence of the estuary drives a dynamic sedimentary regime with accumulation and erosion of sediment in different areas of the tidal flat (van den Berg, 1986; Louters et al., 1998). The intertidal area neighbouring the investigated salt marshes has been experiencing a net erosion of 1–3 cm $year^{-1}$ over the past 23 years. In contrast, the areas adjacent to the intertidal channel have been affected by an accumulation rate of 2–4 cm $year^{-1}$ in the same period (Fig. S2).

The supratidal flat section of the study area has a top aquitard formed by Holocene, marine clay sediments of nearly 1 m thickness. Below this clay-rich layer, a marine, Holocene layer of c. 22 m thickness with predominantly fine sand to clay-rich sand is present across the study area. This layer is followed by a fluvial, Early Pleistocene unit of c. 45 m formed by sand and clay layers. A minor sandy, Late Pleistocene periglacial layer may be present in between. At the bottom, this sequence is limited by an Early Pleistocene, marine clay-rich layer of 1–3 m of thickness, a 20 m thick aquifer below and another 10 m thick Pliocene, marine clay layer (Fig. 2). The supratidal flats in the Eastern Scheldt estuary usually have marsh soils of variable thickness (Oenema and DeLaune, 1988). The accretion rates at the Krabbenkreek salt marsh were measured by Ma et al. (2014). They observed accretion rates that vary between 1.22 and 10.74 mm $year^{-1}$. The highest accumulation rates were observed at the creek levees (5.80–10.74 mm $year^{-1}$), while mean accretion rates in the middle marsh were slightly higher than those in the high marsh areas.

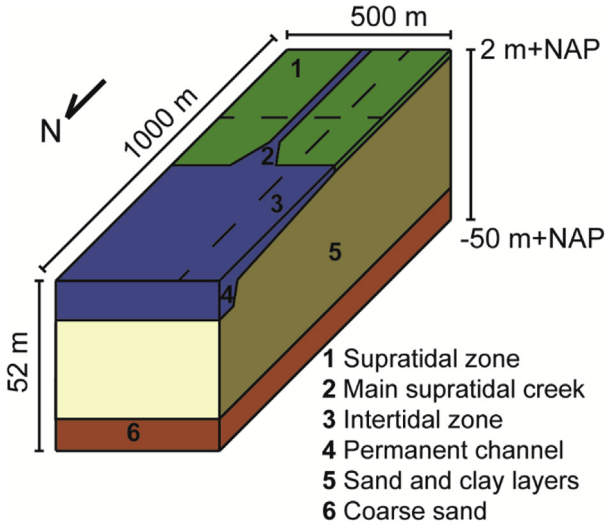

Fig. 2. The sub-environments modelled in this study and their dimensions (where m + NAP refers to the Dutch Ordnance Datum, similar to Mean Sea Level). Dashed lines correspond to the lateral and perpendicular profiles of the model domain. The domain was composed by no flow boundary conditions at the bottom and east and west boundaries, a permanent channel at the north boundary and a general head boundary (GHB) in the south. The top 1 m of the supratidal zone (1) corresponds to the aquitard.

2.2. Field campaigns

2.2.1. Sediment sample collection

Sediment samples from the supratidal and intertidal flats were collected from 13 drilling locations along several transects perpendicular to the creeks. These drillings were located in the middle and high marsh areas of the supratidal flat and at the boundary between the intertidal and supratidal flat (Fig. 1). The transects in the marsh area started next to creeks while the transect on the intertidal flat started near the cliff of the supratidal flat and ended next to a draining creek coming from the supratidal flat. The drillings were carried out with an Eijkelkamp hand auger and samples were collected every 0.5 or 1 m with a 25 cm long Akkerman core sampler tube (Eijkelkamp) starting at 0.5 m depth. The drillings reached depths that varied between 3 and 5 m below ground surface (m.b.g.s). The Akkerman tubes were sealed with metal cylinders and plastic lids. Later, the samples were stored under anoxic conditions after sampling completion and transportation to the laboratory (24–48 h after sample collection).

2.2.2. Piezometer construction and installation

Eleven piezometers were installed in the intertidal and supratidal flats to monitor the groundwater levels during 7 days. The piezometers were placed in two different transects to follow the groundwater patterns in different sections of the study site (Fig. 1) in response to oscillating seawater levels. The first transect was located at the high marsh area of the supratidal flat. This transect focused on investigating the temporal variations of the groundwater head and the vertical ranges with respect to the distance from the creek. The second transect was located along the intertidal to supratidal flat (Fig. 1). This transect focused on constraining the hydraulic potentials along the transition from the intertidal to supratidal flats.

The borehole drilling for the piezometer installation was carried out with an Eijkelkamp hand auger for the upper meter and continued with an Eijkelkamp bailer boring auger in the deeper water-saturated sections. The piezometers consisted of 4 cm diameter PVC pipes, covered with a nylon sock at the screen. All the piezometer screens were located at the bottom of the borehole. The depth of the boreholes varied with respect to the location. The borehole installed in the creek at the high marsh part of the supratidal flat was 0.5 m depth, while the adjacent boreholes ranged between 2.5 and 5 m depth. At the intertidal area, the borehole depths were 4 m and near the cliff of the supratidal area the depth varied between 4 and 5 m. All piezometers were installed in October, 2013. In the piezometers, conductivity, temperature and groundwater levels were measured every 5 min using an Eijkelkamp microdiver data logger with a pressure sensor. An extra diver was installed for air pressure correction.

2.3. Sample characterization

Wet sediment samples were collected from the central part of the Akkerman tubes in an Ar-filled glove box. Porewater was extracted by centrifuge separation using 50 ml maxi-spin tubes with a 0.45 μm maxi-spin nylon centrifugal filter of 25 ml. Afterwards, the centrifuge tubes were returned into the glove box and the porewater was retrieved. The pH and conductivity were measured inside the glove box and the samples were subsequently split into two subsamples. The first subsample was used to determine SO_4 and Cl concentrations with ion chromatography (IC) and for isotope (δD and $\delta^{18}O$) analysis. The detection limits for NO_3, SO_4 and Cl were 84, 51 and 32 mg/l for saline water, respectively. The coefficients of variation of triplicate measurements of δD and $\delta^{18}O$ isotopes were $\leq 2‰$ and $\leq 0.1‰$, respectively. The averaged fresh water $\delta^{18}O$ and δD isotopes from rain in Zeeland ($\delta^{18}O = -6.7‰$; $\delta D = -43.6‰$) and the Rhine river

($\delta^{18}O = -9.2‰$; $\delta D = -65.8‰$) were provided by the Centre for Isotope Research of Groningen University. The second series of subsamples was acidified with 32% HCl to pH below 2, stored at 4 °C and later analysed for major and trace elements with ICP-OES and ICP-MS, respectively. Porewater chemistry was compared to data of stations in the Eastern Scheldt from the Executive Agency of the Ministry of Infrastructure and Water Management of the Netherlands (live.waterbase.nl).

The remaining sediment was freeze dried and elemental composition was determined by total digestion in a mixture of 2.5 ml HF and 2.5 ml 3:2 $HClO_4$:HNO_3 and later analysed by ICP-OES. Total carbon and total sulphur contents were determined by CS analysis (LECO CS-632). Detection limits for total carbon and sulphur are 0.005% and 0.001%, respectively. The CS analyses have a relative standard deviation (RSD) of 1% for both total carbon and total sulphur. The C_{org} was determined by CN analyses (Fisons NA 1500 NCS) using decalcified yields. The detection limit for the C_{org} is 0.001% with a typical precision of 0.5%, when the contents are below 0.01% the standard deviation can reach up to 10%. The inorganic carbon ($C_{inorganic}$) was calculated from the difference between the total and C_{org}. The mineralogical composition of several samples was analysed by X-ray diffraction (XRD) using a Bruker D2 instrument equipped with a Co tube. Mineralogical identification and quantification of both bulk and clay phases was done on a sample by XRD Rietveld refinement at Qmineral laboratory.

For grain size distribution analysis of the sediments, freeze dried samples were pre-treated with 15% H_2O_2 and 0.5% HCl solutions for the removal of OM and carbonates and then suspended in 1% $Na_4P_2O_7{\cdot}10H_2O$. Subsequently, the particle size distribution was determined with a particle size analyser based on static laser diffraction Helos KR (Sympatec). The sediments of the supratidal and intertidal flats were classified according to their grain size distribution based on the textural classification proposed by Flemming (2000).

Iron speciation was determined based on the method developed by Claff et al. (2010) and Mehra and Jackson (1958). Here, 5 extraction steps (Fe_{HCl}, Fe_{org}, Fe_{CDB}, Fe_{HNO3} and Fe_{res}) were performed (Table S1). The Fe(II) fraction from the HCl step was determined colorimetrically using ferrozine according to the protocol described by Viollier et al. (2000). The reactive Fe ($Fe_{reactive}$) pool is formed by the sum of the extracted Fe in the first four steps (Fe_{HCl}, Fe_{org}, Fe_{CDB} and Fe_{HNO3}). The reactive Fe(II) phases correspond to the sum of $Fe(II)_{HCl}$ and Fe_{HNO3}, while the reactive Fe(III) pool is represented by the combination of $Fe(III)_{HCl}$ and Fe_{CDB}. Molybdenum (Mo) content from pyrite was obtained by evaporating 5 ml of the extracted concentrated nitric acid (fourth step) at 120 °C in a hot plate until it was almost dried and then added 10 ml of 0.1 M ultra pure HNO_3 and later diluted tenfold.

Acid volatile sulphide (AVS) was determined based on the method described by Burton et al. (2008). The deviations between duplicates for Fe and AVS extractions were ≤ 5 and $\leq 8\%$, respectively. For samples with S contents below 0.01%, the maximum deviation reached 10%. The actual pyrite content was calculated by correcting the Fe_{HNO3} extraction results for the dissolution of clay minerals. This was done based on the measured Al concentration by assuming a molar Fe:Al ratio of 1:4, based on the work of Huisman and Kiden (1998), Dellwig et al. (2002) and Rudnick and Gao (2003).

2.4. Hydrogeological modelling

A conceptual model was applied to study the influence of tidal fluctuations on the groundwater flow in the supratidal/intertidal flat. A schematic diagram representing the conceptual model is presented in Fig. 2 (for domain grid details see Table S2). The model was built using the three-dimensional (3D) finite-difference groundwater model MODFLOW under transient flow conditions (for model parameters see Supplementary Table S3). The northern boundary of the domain corresponded to a permanent water channel (Fig. 2). The model had no-flow boundaries at the sides and at the bottom of the domain, and a general head boundary (GHB) at the south of the domain to simulate the groundwater level at the polder area. The creek and the surface of the intertidal flat were considered river surfaces and their riverbed hydraulic conductance (C_{riv}) was estimated. The aquifer medium was assumed to be heterogeneous and 18 layers were defined based on field observations and data from the national hydrogeological model schematisation REGIS II (www.dinoloket.nl).

The model consisted of an upper clay layer of 1 m thickness (layers 1 and 2) for the zone with the supratidal flats. Based on the REGIS II database, the underlying layers had an increasing sand content with depth. Precipitation and incidental seawater flooding by storms were not considered in this model. The impact of both events and their interplay on infiltration in the swampy supratidal flats are hard to foresee and would require a separate field and model study (Andersen et al., 2005; Bear and Cheng, 2010; Jun et al., 2013). Thus, the related model assumption is that both rain and incidental flood water disappear as overland flow out of the model domain. This seems a reasonable assumption considering the poor permeability of the clay-rich top layer in the supratidal flats would result in perching and horizontal flow to a surface drain (Sophocleous, 2004) and therefore in negligible recharge. Before introducing the tide oscillations, the initial heads were equilibrated (*stabilised* in MODFLOW jargon) for 100 years, represented in one time step including 20 subsequent stress periods. Later, the tide fluctuations were investigated for 3 days, represented in 24 time steps of 3 h each.

The model fitting involved parameters such as the horizontal hydraulic conductivity (k_h), vertical hydraulic conductivity (k_v) and effective porosity (Table S3). The optimized k_h values are in the same order of magnitude as the permeability test results and in the ranges suggested by REGIS II. The assigned k_h and effective porosity values are comparable with those values reported for other marsh areas (e.g. Gardner, 2005; Wilson and Gardner (2006); Xia and Li, 2012).

The model was assessed by comparing simulated heads and tide-to-tide head gradients with those observed in the field area (Fig. S3). After calibration, the maximum difference between modelled heads and averaged field heads during high and low tides was less than 20 cm.

3. Results

3.1. Groundwater flow patterns

The semi-diurnal tides with a tidal range of nearly 3 m were translated into a wide range of hydraulic head fluctuations, which are well reproduced by the calibrated model (Fig. S3). At ebb tide, hydraulic gradients steepened in the study area, as the amplitude of the oscillating hydraulic heads decreased with increasing distance from the permanent channel. In the marsh areas, hydraulic head fluctuations were ~0.5 m, with the exception of the area near the cliff (0.9 m). The highest oscillations were present in the intertidal area (~1.5 m). High tide hydraulic heads were nearly similar in all piezometers (Fig. S3), leading to a difference in hydraulic head between high marsh and intertidal flat of only 0.3 m.

Groundwater velocities were 1–2 orders of magnitude larger at low tide than at high tide (Fig. 3). The predominant groundwater flow occurs during low tide from south to north in the supratidal flat and upwards in the intertidal flat (Fig. 3). High tide periods are characterized by seawater infiltration, while during low tide groundwater seepage is observed. This groundwater flow pattern is consistent with those reported by Gardner (2005), Wilson and Gardner (2006) and Xia and Li (2012) in similar tidal environments.

The upper section of the model domain comprises the soil of the supratidal marsh, which includes a 1 m clay layer at the top that acts as an aquitard. This layer exerts a major influence on the hydrodynamics of the whole system. In this aquitard, flow velocities are very low (Fig. 3). Here, the flow velocities vary between 10^{-13} at high tide to 10^{-9} m s^{-1} at low tide (in the cliff area) (Fig. 3A and B). In contrast, the

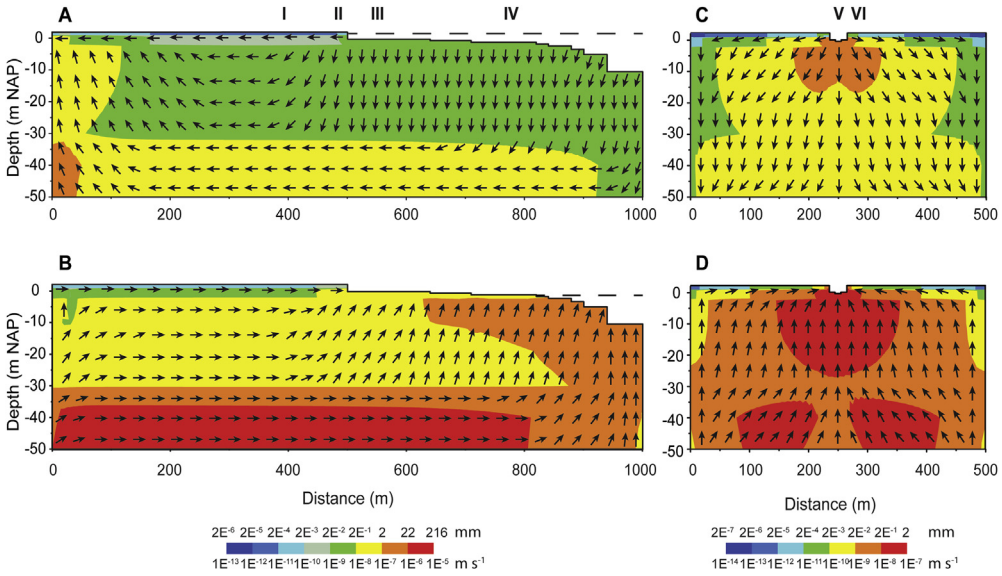

Fig. 3. Flow velocities (in m/s) in the intertidal/supratidal area transect during (**A**) high tide and (**B**) low tide with flow velocities (in m/s) at the perpendicular section of the supratidal area during high tide (**C**) and low tide (**D**). The colour contours represent the magnitude of flow velocity (m/s) and the related travel distance in half a tide time, i.e., in 6 h. The arrows show the flow vectors and the dashed line represents the surface water level. The roman numbers indicate the locations for travel time calculations presented in Table S4. (For interpretation of the references to colour in this figure legend, the reader is referred to the Web version of this article.)

flow velocities in the underlying sandier sediments (1–2 m) range between 10^{-10} (at high tide) and 10^{-7} m s^{-1} (at low tide, cliff area) (Fig. 3A and B).

The flow velocities the middle section of the domain (0 to −37 m + NAP (which corresponds to the Dutch Ordnance Datum, similar to Mean Sea Level, positive values are above the standard reference point and negative values are below)) (Fig. 3A and B) vary from 10^{-9} to 10^{-6} m s^{-1} between tide ends (considers lateral variations). Flow velocities are higher in the intertidal flat compared to the supratidal flat. Furthermore, groundwater flow velocities are enhanced in the vicinity of the permanent channel due to convergence of flow (Fig. 3A and B). This is consistent with findings by Wilson and Gardner (2006), who report considerable groundwater flow towards intertidal creeks during low tide. Gardner (2005) also found that the intensity of the flow towards the channel depends on the slope of the creek banks and increases with higher slope.

Due to the vertical differences in hydraulic conductivity, the groundwater flow velocity is considerably higher in the deeper part (−37 to −50 m + NAP) of the domain (Fig. 3A and B), with velocities that vary between 10^{-9} (near the permanent channel) and 10^{-5} m s^{-1} (supratidal/intertidal zone) during high and low tides, respectively.

The supratidal creeks have a major impact on the groundwater flow in the supratidal flat by enhancing the infiltration and drainage through the bottom and sides of the creek (Fig. 3C and D). The presence of the supratidal creeks induces a flow component that is perpendicular to the creek and vertical flow component at the bottom of the creek. The groundwater flow velocities close to the bottom of the supratidal creek vary between 10^{-9} to 10^{-7} m s^{-1} (Fig. 3C and D). The groundwater velocities in the sandy sediments that underlay the aquitard usually vary between 10^{-12} m s^{-1} at high tide (in the edges of the domain) to 10^{-7} m s^{-1} at low tide (in the vicinities of the creek), with the highest flow velocities present in the immediate surroundings of the supratidal creek (10^{-9} to 10^{-7} m s^{-1}) (Fig. 3C and D).

The observed low groundwater flow velocities are translated into travel times for a few meters that vary between centuries (aquitard and sands below aquitard) to several years (intertidal zone, near the permanent channel) (Table S4).

3.2. Sediment

3.2.1. Particle size distribution: textural differences

The sediments are in four textural groups: sandy muds (50–75% mud; n = 3), muddy sands (25–50% mud; n = 13), slightly muddy sands (5–25% mud; n = 38) and sands (< 5% mud; n = 17), where mud is defined as the clay plus silt fraction. For practical purposes, the sediments were divided into two main groups, based on mud content: 1) mud-rich sediments (> 25% mud) and 2) sand-rich sediments (< 25% mud). This classification reflects the major local textural trends in the supratidal and intertidal flats (Fig. 4A).

The supratidal flat as represented by the high and middle marsh transects (Fig. 4A), contain mud-rich upper sediments near the surface that are overlaying sand-rich sediments. According to the textural classification, 65% of the upper sediment samples from the supratidal area correspond to mud-rich sediments (Fig. 4A). The mud content in the upper sediments varies laterally (Fig. 4A): the mud content increases with increasing distance from the creek in the high marsh area (B1 in Fig. 4) while in the middle marsh area the upper sediments are either mud-rich (B2 in Fig. 4) or sand-rich (B3 in Fig. 4). The mud-rich sediments in the levees (L1 and L2 flats Fig. 4) comprise 1–1.5 m of thickness. In this area, the levees have higher accretion rates (2.9–8.8 times) when compared to the back marsh areas (Oenema and DeLaune, 1988; Ma et al., 2014) which explains the formation of thicker mud-rich layers near the creeks.

The intertidal flat is dominated by sand-rich sediments with common occurrence of mud-rich sediments in the upper section at the upslope and downslope areas (Fig. 4A). The upslope area (I1 in Fig. 4) has the highest mud content (34%) closest to the cliff of the supratidal flat. According to de Jong et al. (1994), the supratidal edges of the Eastern Scheldt estuary are under constant erosion. This suggests that the erosion could lead to the accumulation of mud in the intertidal sediments located near the cliff of the supratidal flat.

3.2.2. Organic carbon and total sulphur content

In the supratidal flat, the mud-rich samples of the middle marsh transect have nearly 2 times higher total sulphur (S_{total}) contents than the related sand-rich sediments (Fig. 5A), while the sediments of the high marsh transect have comparable S_{total} contents (~0.03 mmol g^{-1}) in both the mud-rich and sand-rich sediments (Fig. 5A). The C_{org} content is higher in the middle marsh transect (0.11–1.12 mmol g^{-1}) when compared to the high marsh transect (0.07–0.83 mmol g^{-1}) (Fig. 5A). The mud-rich sediments in the levees (L1 and L2 flats Fig. 4) are characterized by high C_{org} (0.39–0.68 mmol g^{-1}) contents when compared to the surrounding mud-rich supratidal sediments. In the intertidal flat, the C_{org} and S_{total} contents in the upper mud-rich sediments are nearly 6 and 4 times higher than in the sand-rich sediments, respectively (Fig. 5A).

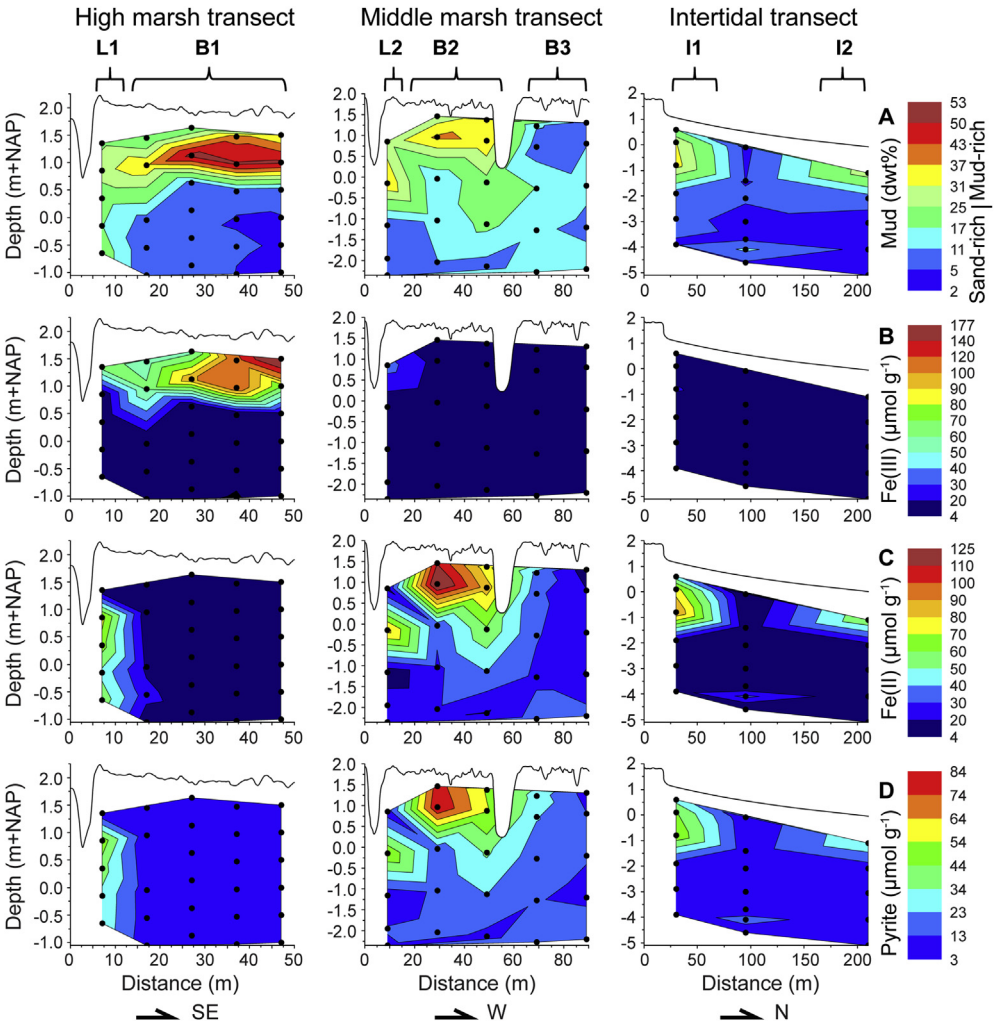

Fig. 4. Distribution of **A**) Mud content, **B**) Fe(III) content, **C**) Fe(II) content and **D**) Pyrite content in the sediments of the different transects. Black dots show the sampling locations.

3.2.3. Iron speciation

3.2.3.1. Intertidal and middle marsh sediments. Iron contents and their distribution over different Fe fractions are similar in the corresponding mud-rich and sand-rich sediments of the intertidal flat and middle marsh transect. In the $Fe_{reactive}$ pool, Fe(II) is generally more abundant than Fe(III). In the sand-rich sediments, the contribution of Fe(III) tends to be larger than in the mud-rich sediments, although the mud-rich sediments are generally located closer to the sediment/water and sediment/atmosphere interfaces. These reactive Fe(III) phases are mainly in the form of crystalline iron oxides (Fig. 5C). Most of the Fe (II) containing $Fe_{reactive}$ is in the form of pyrite (Fe_{HNO3}) which is also the largest $Fe_{reactive}$ pool in these sediments. The pyrite contents in these sediments vary between 0.02 and 0.47%, which is translated into 34–58% of the $Fe_{reactive}$. Molybdenum extracted with the concentrated HNO_3 correlates with the Fe from pyrite (Fig. S4), which suggest that pyrite is an important source of Mo.

AVS was only detected in few samples with contents below 4 µmol g^{-1}. The lack of AVS in these sediments, as well as the positive

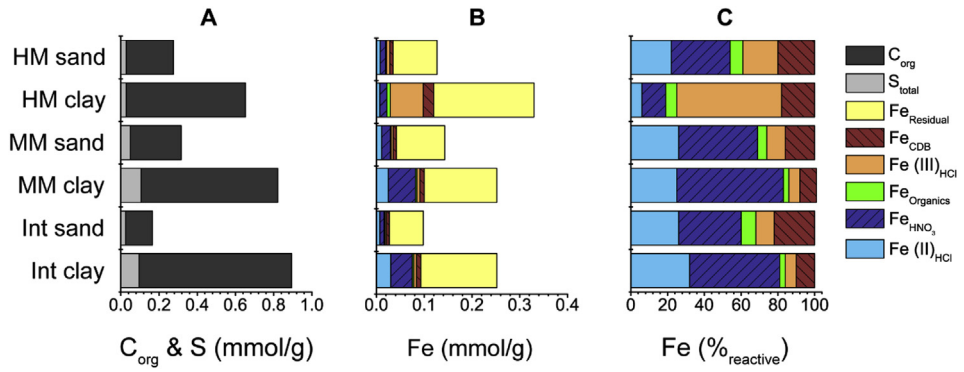

Fig. 5. Average sediment composition for the distinguished sample types: **A**) organic carbon and sulphur contents and **B**) Fe contents and **C**) distribution of reactive Fe.

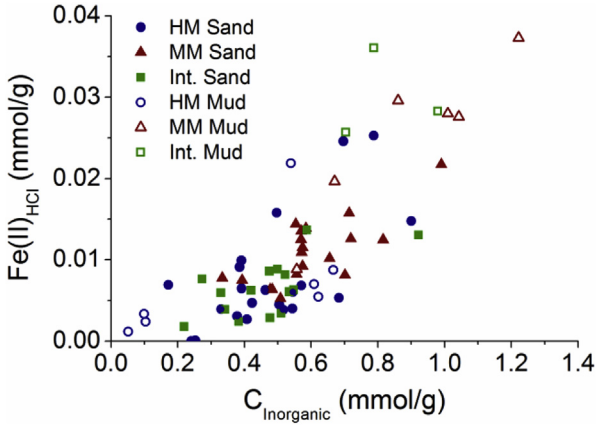

Fig. 6. Inorganic carbon ($C_{inorganic}$) contents vs. the $Fe(II)_{HCl}$ content of the sediment samples (HM is high marsh, MM is middle marsh and Int. is intertidal flat).

correlation of $Fe(II)_{HCl}$ with calcium carbonates (Fig. 6), suggests that Fe-bearing carbonates are the second most important reactive Fe(II) phase. The presence of ankerites was confirmed by XRD analysis, which reported 0.8% of ankerites in a sample from the middle marsh area (data not shown).

3.2.3.2. High marsh sediments. The sediments in the high marsh transect are characterized by a higher content of Fe(III) phases than in the middle marsh transect or the intertidal flat. In contrast to the middle marsh and intertidal sediments, the $Fe_{reactive}$ pool of the mud-rich upper sediments in the high marsh sediments are predominantly formed by Fe(III) phases (82 ± 4% of the $Fe_{reactive}$) (Fig. 5C), while the underlying sand-rich sediments have an Fe(III) fraction that is around 25 ± 8% of the $Fe_{reactive}$ pool (Fig. 5C).

3.3. Groundwater chemistry

The groundwater of the supratidal and intertidal flats is mainly saline according to the classification criteria of the Venice system (1958). Chloride concentrations in the porewater of intertidal and supratidal sediments vary between 360 and 515 mM (Fig. 7A), where the Cl concentrations are usually above 420 mM. The mean Cl concentration in the Eastern Scheldt estuary is 500 ± 20 mM (live.waterbase.nl). Areas with low Cl concentrations are found near the creeks of the supratidal flat and in the downslope part of the intertidal flat. The differences in $\delta^{18}O$ and δD of the rain water and Rhine river water provide a possibility to distinguish between the two potential fresh water sources. However, the seawater component in all waters is high and, consequently, the difference between the mixing lines is too small, when compared to the bulk data, to allow an unequivocal identification of the dominant fresh water source (Fig. S5).

The SO_4 to Cl molar ratios in most groundwater samples exceed those in the Eastern Scheldt estuary (0.045 ± 0.005) (live.waterbase.nl) (Fig. 7B). In the supratidal flat, high sulphate enrichments (SO_4 to Cl ratios of 0.07–0.10) are observed in the deeper, sand-rich sediments of the high and middle marsh areas (Figs. 4A and 7B). The B3 area of the middle marsh area has SO_4 to Cl ratios that reach 0.12 (Fig. 7B). The high SO_4 concentrations in this transect are found from shallow (~1.5 m + NAP) to deep (~−2 m + NAP) depths. In the intertidal flat, high SO_4 to Cl ratios (≥0.07) are mostly observed at shallow depths. Nitrate concentrations were below detection limit.

High Ca concentrations coincide with elevated SO_4 to Cl ratios in the middle marsh and the intertidal transects (Fig. 7B). The highest Ca concentrations (17–27 mM) are present in the B3 area of the middle marsh transect (B3 flat, Fig. 7C). Despite the high Ca and SO_4 concentrations, solutions are undersaturated with respect to gypsum.

The Mo concentrations in the groundwater of the deeper sediments of transect HM and of the B3 section of transect MM exceed those in local seawater (0.11 μM) (live.waterbase.nl). The groundwater at these locations is also characterized by generally elevated SO_4 to Cl molar ratios. A hot spot with Mo concentrations that reach 9.89 μM is located adjacent to the creek (L1, Fig. 7D) in the high marsh transect. The maximum concentrations are found at the transition from sediments with relatively high Fe(III) content to those with elevated Fe(II) (Fig. 4).

Dissolved Fe concentrations only exceed the detection limit in a few samples (Fig. 7E). The detected Fe concentrations range between 0.99 and 1.75 μM while the Eastern Scheldt estuary water has a filtered average Fe concentration of 4.78 ± 4.43 μM (live.waterbase.nl).

Groundwater concentrations of Mn exceed the average concentration of the estuarine water (0.27 ± 0.14 μM) (live.waterbase.nl) (Fig. 7E). The high marsh area has the lowest Mn concentrations, which vary between 0.16 and 6.49 μM with one outlier of 7.93 μM (Fig. 7E). In contrast, the porewater in the middle marsh area reaches up to 52 μM. The highest Mn concentration is located in the deep section of the B3 flat (Fig. 7E). In the intertidal flat, Mn concentrations decrease downslope, reaching a maximum concentration of 16 μM.

4. Discussion

4.1. Groundwater flow

Analysis of the flow patterns, obtained from the groundwater model, indicates that water flows predominately horizontally below the supratidal flat and vertical water movement only occurred below the intertidal flat. Although the groundwater flow patterns are consistent with those reported in similar tidal environments, the flow velocities at both high and low tides are lower. Consequently, the slow groundwater flow observed in the deep sediments of the supratidal and intertidal flats at the Krabbenkreek is translated into a very limited convective transport of dissolved constituents.

In general, marshes and intertidal flats are characterized by vertical redox gradients. The observed groundwater flow, in turn, suggests that there is no significant convective transport of dissolved Fe and other elements with redox sensitive mobility across redox boundaries below the supratidal flat and deep sediments of the intertidal flat at Krabbenkreek.

Pronounced oscillating groundwater flow can lead to mixing zones in subterranean estuaries and the development of strong Fe enrichments (Robinson et al., 2007). The groundwater model suggests that this driving force for enrichment of Fe at subsurface redox boundaries is relatively weak at the Krabbenkreek.

4.2. Redox dynamics of Fe

The Krabbenkreek tidal flat presents absent to negligible dissolved Fe concentrations in the interstitial porewater of deep sediments. In this type of setting, elevated concentrations of dissolved Fe in porewater is usually the product of pyrite oxidation (Oenema, 1990a) or Fe oxide reduction driven by OM mineralisation (Oenema, 1988). At the Krabbenkreek, none of these two processes appears to cause substantial mobilization of Fe in the groundwater-saturated zone.

4.2.1. Preservation of Fe oxides

Presence of bioavailable Fe oxides is a prerequisite for Fe mobilization by microbial Fe reduction (Hacherl et al., 2001). At the high marsh, poorly crystalline Fe oxides are the dominant form of reactive Fe in the mud-rich layer down to 1.5 m.b.g.s. Poorly crystalline Fe oxides are suitable substrates for microbial Fe reduction, implying that the respiratory activity in the mud-rich part of the high marsh is not high enough to induce Fe reduction.

The absence of Fe reduction in this part of the marsh might be explained by a combination of two factors. First, sufficient supply of

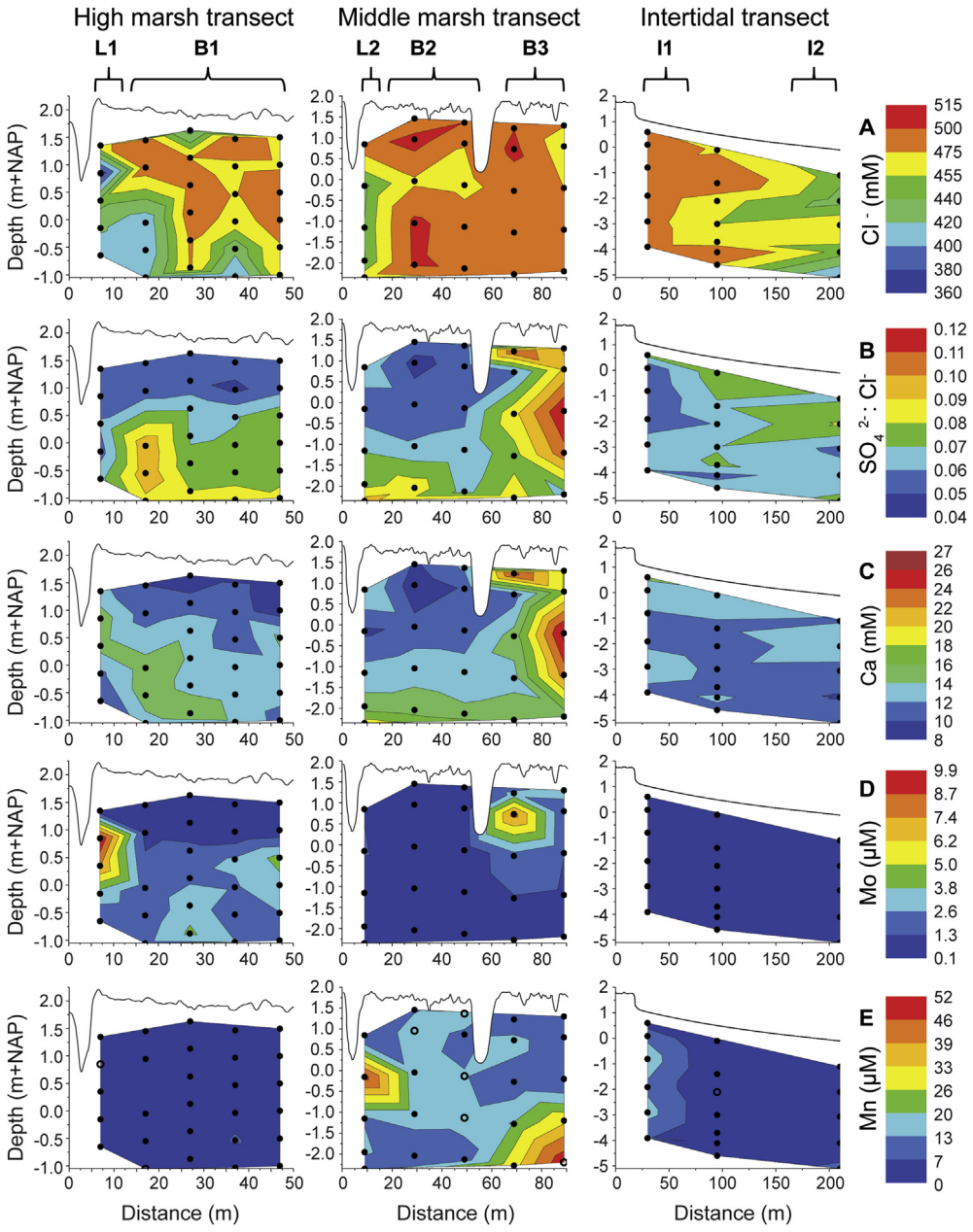

Fig. 7. Composition of porewater along the different transects of the supratidal/intertidal area: **A**) chloride concentrations, **B**) SO_4 to Cl ratio, **C**) calcium concentrations, **D**) molybdenum concentrations and **E**) manganese concentrations. Circles show the position of sampling points; open circles in **(E)** indicate sampling points at which dissolved Fe was above detection limit.

electron acceptors with higher redox potential than Fe oxides can be reason for limited Fe reduction. Measured nitrate concentrations were below detection limit and molecular diffusion of oxygen is not a very effective transport mechanism. However, aeration of the sediments in the high march can be caused by episodic events such as desiccation of the salt marsh soils and strong burrowing activities of mice and rabbits (de Jong et al., 1994) and by this keeping the Fe oxides in their oxidized state.

Second, the long term preservation of Fe oxides might only be possible when microbial respiration is also limited by the availability of OM. The measured C_{org} contents in the mud-rich sediments are low compared to other areas in the Scheldt. Also, Oenema (1988) found that the OM in subrecent sediments is mainly refractory. He concluded that this deposited refractory OM is the remnant of OM which has been subjected to 3–4 centuries of mineralisation during transport, involving repeated cycles or resuspension and deposition. Also, reworking of sediment can lead to repeated exposure of the sedimentary OM to dissolved oxygen and its progressive degradation (Hartog et al., 2004, 2005; Middelburg and Herman, 2007). The low conductivity of the surficial layer can account for the restricted supply of fresh, reactive dissolved C_{org}, produced by the decay of plant and root material at the supratidal marsh, to the underlying sediments. Due to the lacking provision of fresh OM, the availability of electron donors is too low to reverse the periodic oxidation of Fe(II) leading to a long term conversion of reactive Fe(II) into reactive Fe(III) phases in the high marsh, even when water saturation prevails. This conclusion is an outcome of the hydraulic model and is supported by the small freshwater fraction in the analysed groundwaters. This means that infiltration of water, which could percolate through the soil and could leach dissolved OM into deeper parts of the sediment, is very low. Hence, the sediments most likely contain predominantly refractory OM with low potential to drive early diagenesis in the sediments.

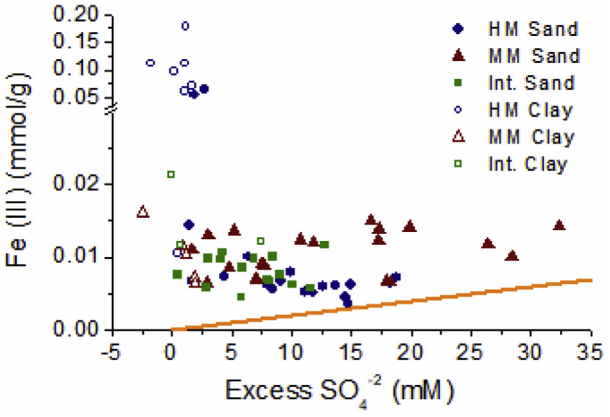

Fig. 8. Comparison of Fe (III) sediment contents with excess sulphate concentrations in porewater from the same sampling location. The orange line represents the amount of Fe(III) which would be formed stoichiometrically when all the excess SO_4 was produced by pyrite oxidation. (HM is high marsh, MM is middle marsh and Int. is intertidal flat). (For interpretation of the references to colour in this figure legend, the reader is referred to the Web version of this article.)

4.2.2. Origin of Fe oxides

Fe oxides in the marsh can be of authigenic or allochthonous origin. Poorly crystalline Fe oxides are only metastable and tend to convert into crystalline Fe oxides (Drits et al., 1993; Schwertmann et al., 1999; Cornell & Schwertmann, 2003). Hence, the prevalence of poorly crystalline Fe oxides indicates that the Fe(III) phases have relatively recently been formed (Jambor and Dutrizac, 1998; Cornell & Schwertmann, 2003) and are consequently a product of diagenetic processes. A likely pathway for the formation of Fe oxides in these sediments is the oxidation of Fe(II) containing phases, in particular pyrite.

Oenema (1988) reported that the release of oxygen in the rhizosphere can cause oxidation of pyrite and can lead to the concomitant formation of Fe oxides. Oxidation of pyrite in sediments is accompanied by an enrichment of the porewater in SO_4 (Oenema, 1990a). The relatively low SO_4 to Cl ratios in the groundwater of the mud-rich layer of the high marsh (Fig. 7B) indicate that oxidation of pyrite is not a current process in these sediments. In general, the excess SO_4 in the groundwater was not translated into a detectable increase in Fe oxide content (Fig. 8) as the Fe(III) content was considerably higher than the recent formation of Fe oxides by pyrite oxidation.

In the high marsh area, temporary pyrite oxidation can be explained by episodic aeration periods. Another possibility is the formation of Fe oxides when allochthonous pyrite is deposited on the high marsh. The low sedimentation rates and incidental flooding events (Oenema and DeLaune, 1988; Ma et al., 2014) allow the sediments to become oxidized as they accrete in this area. In summary, the observed high Fe oxide contents in these sediments are likely the result of pyrite oxidation during accretion of the suspended matter and episodic dry periods in which aeration of the subsurface sediments was enabled. These events can also explain the preservation of the buried Fe oxides in combination with low rates of OM mineralisation.

4.2.3. Pyrite oxidation

Porewater chemistry indicates ongoing pyrite oxidation in the sand-rich sediments. Excess of SO_4, Ca and Mo in the porewater points to oxidation of Mo-bearing pyrite in the supratidal and intertidal flats. This is in agreement with porewater chemistry reported in other tidal flats, where high SO_4 concentrations related to sulphide oxidation were reported (Kolditz et al., 2009). The concurrence of excess SO_4 with elevated Mo concentrations in groundwater supports the interpretation that pyrite oxidation is an ongoing process in the sand-rich sediments. Iron sulphides and ultimately pyrite are major sinks for Mo in marine settings (Kuroda and Sandell, 1954; Vorlicek et al., 2004; Bostick et al., 2003). Hence, oxidation from Mo-bearing pyrites in salt marsh areas results in increasing Mo concentrations in porewater (Wang et al., 2011). Sulphur isotopes may be useful in identifying the definite source for the excess sulphate in the groundwater of the sand-rich sediments.

The correlation between excess concentrations of SO_4 and Ca indicates that the production of protons from the oxidation is buffered by calcium carbonate dissolution. Despite pyrite oxidation, the porewaters remains slightly alkaline due to Ca carbonate buffering the pH (Fig. S6). The increase in SO_4 and Ca in the porewater can induce gypsum formation which has been reported as a product of pyrite oxidation associated with carbonate weathering (Ritsema and Groenenberg, 1993). Thermodynamic calculations show that all groundwater samples are undersaturated with gypsum and XRD results do not provide evidence for the presence of gypsum in the sediments (data not shown). At low pH, Fe(II) released from pyrite during oxidation can be metastable due to low abiotic oxidation kinetics (Rimstidt and Vaughan, 2003). At neutral and slightly alkaline pH, Fe(II) oxidation proceeds very fast and is followed by instantaneous precipitation of Fe oxides. In other words, oxidation causes an in situ transformation of pyrite into Fe oxides and does not contribute to Fe transport and enrichment in these sediments.

4.2.4. Origin of pyrite

The absence of AVS suggests that there is little or no ongoing authigenic formation of iron sulphides in the sediments; as sulphidisation of iron oxides is the most common process for AVS formation (Rickard and Luther, 2007). This suggest that pyrite in these sediments is predominately of allochthonous origin. Pyrite has been reported to be present in the suspended matter of the Eastern Scheldt estuary. The suspended matter is the result from erosion of sediments exposed elsewhere in the Eastern Scheldt (Oenema, 1989). Harmsen (1954) found 0.78% bisulphidic sulphur in suspended marine detritus in Zeeland, while Oenema (1990a) reported 0.5–1% of detrital pyrite in suspended matter filtered from flood currents. This pyrite is commonly fixed to the suspended OM in the estuary system (Kooistra, 1981) and can therefore explain the correlation between C_{org} and pyrite content. This conclusion implies that also the pyrite in the Krabbenkreek sediments is predominately of allochthonous origin. The pyrite contents present in the intertidal and deep supratidal sediments (0.02–0.47 dw %) are in agreement with the detrital pyrite content of suspended material in tidal currents and do not represent the enrichments (3–6 dw %) present in the Naaldwijk formation (van Gaans et al., 2011; Griffioen et al., 2012).

4.3. Comparison of the Krabbenkreek tidal flat with other tidal flats

The biogeochemical dynamics of Fe in the deep sediments of the Krabbenkreek tidal flat is unusual and deviates from most other investigated tidal wetlands. Deep sediments in tidal wetlands are often characterized by high biogeochemical Fe dynamics driven by tidally induced water exchange between sediments and surface water (Billerbeck et al., 2006; Wilson and Gardner, 2006), high input of reactive OM (Postma, 1981; Kowalski et al., 2009) and presence of high amounts of reactive Fe (Cutter and Velinsky, 1988; Charette and Sholkovitz, 2002; Johnston et al., 2011). Typically, microbial sulphate reduction promotes formation of iron sulphides in the deeper parts of tidal sediments (Beck et al., 2008b; Johnston et al., 2009; Beck & Brumsak, 2012). Deviating from this general pattern, indications for ongoing oxidation of iron sulphides is a common feature in the Krabbenkreek. Main reasons for this deviating behaviour might be the low reactivity of the OM (Oenema, 1988) and the limited water exchange due to the low permeability of the surficial layer of the supratidal sediments.

This study demonstrates that the enhanced biogeochemical activity in coastal wetlands, as reported in many studies (eg. Charette and Sholkovitz, 2002; Beck et al., 2008a; Johnston et al., 2011; Mazumdar et al., 2012) is not a general feature of these environments. The sluggish

redox cycling of the Fe in the Krabbenkreek tidal flat highly contrasts with that in other tidal flats such as Spiekeroog Island and Waquoit Bay where the hydrodynamics act as a trigger for active redox transformations of Fe. In the Wadden Sea, advective groundwater flow maintains the nutrient supply for enhanced mineralisation of OM (Beck & Brumsak, 2012) that often results in the formation of pyrite (Beck et al., 2011). In another example, the tidal sediments from the Waquoit Bay show enrichments of iron oxides in the deep sands (Charette and Sholkovitz, 2002) due to the mixing of Fe^{2+}-bearing groundwater with oxygenated seawater (Charette et al., 2005).

5. Conclusions

The Krabbenkreek tidal flat presents clear hydrologic and geochemical zonations across the supratidal/intertidal area. Groundwater Cl concentrations are in general somewhat lower than seawater concentration indicating limited infiltration of rain or river water. The Fe geochemistry indicates that the Fe contents follow similar trends as the C_{org} and S_{total} contents where mud-rich sediments of the intertidal flat contain 3 - 4 times higher contents than the sand-rich sediments. In the supratidal flat, the mud-rich sediments have nearly 2–3.5 times more Fe than the sand-rich sediments. The variability of the speciation of reactive Fe is limited between the investigated areas: Fe(III) oxides are prevalent in the high marsh sediments while pyrite prevails in the middle marsh and the intertidal sediments. Iron oxides in the mud-rich sediments of the high marsh area are likely formed upon oxidation of allochtonous pyrite throughout the accretion phase of during periodic oxidation events. AVS-associated Fe(II) is remarkably low and the preservation of Fe oxides in the high marsh sediments indicate low rates of OM mineralisation coupled to Fe and SO_4 reduction. The respiratory activity in the sediments is probably limited by the refractory character of the sedimentary OM and limited transport of fresh OM into deeper sediments. The indications for ongoing pyrite oxidation in sand-rich sediments were obtained based on excess SO_4, Ca, and Mo concentrations in the groundwater. Against expectation, we could not find evidence for a significant spatial redistribution of reactive Fe within the investigated area which would be driven by tidally induced oscillating groundwater flow along redox gradients. This implies that tidal variations in the groundwater force field alone do not lead to pronounced local enrichments in reactive Fe, as found, for example, in the Naaldwijk Formation. We suggest that, additionally, sufficient high hydraulic permeability of the sediments at the transition between surface and groundwater plus the input of reactive OM to drive early diagenetic processes are prerequisites to establish an effective sequence of Fe mobilization, transport, and immobilization and to cause local accumulation of reactive Fe.

Acknowledgements

The research described is part of a research project on reactive Fe minerals in Dutch fluvial and marine sediments and financially supported by TNO Geological Survey of the Netherlands. The authors acknowledge Dineke van de Meent, Helen de Waard, Ton Zalm and Arnold van Dijk for their technical and analytical support, Eric van Zanten from the Rijkwaterstaat (Ministry of Infrastructure and Water Management) for providing the bathymetry information of the Eastern Scheldt, and Bert Kers and Harm-Jan Streurman from the Centre for Isotope Research of the University of Groningen for providing the fresh and seawater isotopic signatures of water in the Netherlands.

Appendix A. Supplementary data

Supplementary data to this article can be found online at https://doi.org/10.1016/j.ecss.2019.02.032.

References

Allen, J.R.L., 2000. Morphodynamics of Holocene salt marshes: a review sketch from the Atlantic and Southern North Sea coasts of Europe. Quat. Sci. Rev. 19 (12), 1155–1231. https://doi.org/10.1016/S0277-3791(99)00034-7.

Andersen, M.S., Nyvang, V., Jakobsen, R., Postma, D., 2005. Geochemical processes and solute transport at the seawater/freshwater interface of a sandy aquifer. Geochem. Cosmochim. Acta 69 (16), 3979–3994. https://doi.org/10.1016/j.gca.2005.03.017.

Appelo, C.A.J., Drijver, B., Hekkenberg, R., de Jonge, M., 1999. Modeling in situ iron removal from ground water. Gr. Water 37 (6), 811–817. https://doi.org/10.1111/j.1745-6584.1999.tb01179.x.

Baeyens, W., Panutrakul, S., Elskens, M., Leermakers, M., Navez, J., Monteny, F., 1991. Geochemical processes in muddy and sandy tidal flat sediments. Geo Mar. Lett. 11 (3–4), 188–193. https://doi.org/10.1007/BF02431011.

Bear, J., Cheng, A.H.D., 2010. Modeling groundwater flow and contaminant transport. Springer, Dordrecht, pp. 834. https://doi.org/10.1007/978-1-4020-6682-5.

Beck, M., Brumsack, H.-J., 2012. Biogeochemical cycles in sediment and water column of the Wadden Sea: The example Spiekeroog Island in a regional context. Ocean Coast Manag. 68, 102–113. https://doi.org/10.1016/j.ocecoaman.2012.05.026.

Beck, M., Dellwig, O., Schnetger, B., Brumsak, H.-J., 2008a. Cycling of trace metals (Mn, Fe, Mo, U, V, Cr) in deep porewaters of intertidal flat sediments. Geochem. Cosmochim. Acta 72 (12), 2822–2840. https://doi.org/10.1016/j.gca.2008.04.013.

Beck, M., Dellwig, O., Liebezeit, G., Schnetger, B., Brumsak, H.-J., 2008b. Spatial and seasonal variations of sulphate, dissolved organic carbon, and nutrients in deep porewaters of intertidal flat sediments. Estuar. Coast Shelf Sci. 79 (2), 307–316. https://doi.org/10.1016/j.ecss.2008.04.007.

Beck, M., Köster, J., Engelen, B., Holstein, J.M., Gittel, A., Könneke, M., Riedel, T., Wirtz, K., Cypionka, H., Rullkötter, J., Brumsak, H.-J., 2009. Deep porewater profiles reflect enhanced microbial activity towards tidal flat margins. Ocean Dynam. 59 (2), 371–383. https://doi.org/10.1007/s10236-008-0176-z.

Beck, M., Riedel, T., Graue, J., Köster, J., Kowalski, N., Wu, C.S., Wegener, G., Lipsewers, Y., Freund, H., Böttcher, M.E., Brumsack, H.-J., Cypionka, H., Rullkötter, J., Engelen, B., 2011. Imprint of past and present environmental conditions on microbiology and biogeochemistry of coastal Quaternary sediments. Biogeosciences 8 (1), 55–68. 2011. https://doi.org/10.5194/bg-8-55-2011.

Billerbeck, M., Polerecky, L., Walpersdorf, E., deBeer, D., Huettel, M., 2006. Surficial and deep porewater circulation governs spatial and temporal scales of nutrient recycling in intertidal sand flat sediment. Mar. Ecol. Prog. Ser. 326, 61–76. https://doi.org/10.3354/meps326061.

Bostick, B.C., Fendorf, S., Helz, G.R., 2003. Differential adsorption of molybdate and tetrathiomolybdate on pyrite (FeS_2). Environ. Sci. Technol. 37 (2), 285–291. https://doi.org/10.1021/es0257467.

Burton, E.D., Bush, R.T., Sullivan, L.A., 2006. Acid-volatile sulfide oxidation incoastal flood plain drains: Iron−sulfur cycling and effects on water quality. Environ. Sci. Technol. 40 (4), 1217–1222. https://doi.org/10.1021/es0520058.

Burton, E.D., Sullivan, L.A., Bush, R.T., Johnston, S.G., Keene, A.F., 2008. A simple and inexpensive chromium-reducible sulfur method for acid-sulfate soils. Appl. Geochem. 23 (9), 2759–2766. https://doi.org/10.1016/j.apgeochem.2008.07.007.

Charette, M.A., Sholkovitz, E.R., 2002. Oxidative precipitation of groundwater-derived ferrous iron in the subterranean estuary of a coastal bay. Geophys. Res. Lett. 29 (10) 85-1-85-4. https://doi.org/10.1029/2001GL014512 2002.

Charette, M.A., Sholkovitz, E.R., Hansel, C.M., 2005. Trace element cycling in a subterranean estuary: Part 1. Geochemistry of the permeable sediments. Geochem. Cosmochim. Acta 69 (8), 2095–2109. https://doi.org/10.1016/j.gca.2004.10.024.

Claff, S.R., Sullivan, L.A., Burton, E.D., Bush, R.T., 2010. A sequential extraction procedure for acid sulfate soils: Partitioning of iron. Geoderma 155 (3–4), 224–230. https://doi.org/10.1016/j.geoderma.2009.12.002.

Cornell, R.M., Schwertmann, U., 2003. The iron oxides: Structure, properties, reactions, occurrences and uses, second ed. Wiley-VCH Verlag GmbH & Co, Weinheim. 664 pp. https://doi.org/10.1002/3527602097.

Crerar, D.A., Knox, G.W., Means, J.L., 1979. Biogeochemistry of bog iron in the New Jersey Pine Barrens. Chem. Geol. 24 (1–2), 111–135. https://doi.org/10.1016/0009-2541(79)90016-0.

Cutter, G.A., Velinsky, D.J., 1988. Temporal variations of sedimentary sulfur in a Delaware salt marsh. Mar. Chem. 23 (3–4), 311–327. https://doi.org/10.1016/0304-4203(88)90101-6.

de Jong, D.J., de Jong, Z., Mulder, J.P.M., 1994. Changes in area, geomorphology and sediment nature of salt marshes in the Oosterschelde estuary (SW Netherlands) due to tidal changes. In: In: Nienhuis, P.H., Smaal, A.C. (Eds.), The Oosterschelde Estuary (The Netherlands): A case-study of a changing ecosystem. Developments in Hydrobiology, vol. 97. pp. 303–316. https://doi.org/10.1007/978-94-011-1174-4_23.

Dellwig, O., Böttcher, M.E., Lipinski, M., Brumsak, H.-J., 2002. Trace metals in Holocene coastal peats and their relation to pyrite formation (NW Germany). Chem. Geol. 182 (2–4), 423–442. https://doi.org/10.1016/S0009-2541(01)00335-7.

Drits, V.A., Sakharov, B.A., Salyn, A.L., Manceau, A., 1993. Structural model for ferrihydrite. Clay Miner. 28 (2), 185–207. https://doi.org/10.1180/claymin.1993.028.2.02.

Dutch Ministry of Infrastructure and Water Management. http://live.waterbase.nl/waterbase_wns.cfm?taal=en. Accessed on June 2015.

Flemming, B.W., 2000. A revised textural classification of gravel-free muddy sediments on the basis of ternary diagrams. Cont. Shelf Res. 20 (10–11), 1125–1137. https://doi.org/10.1016/S0278-4343(00)00015-7.

Froelich, P.N., Klinkhammer, G.P., Bender, M.L., Luedtke, N.A., Heath, G.R., Cullen, D., Dauphin, P., Hammond, D., Hartman, B., Maynard, V., 1979. Early oxidation of

organic matter in pelagic sediments of the eastern equatorial Atlantic: suboxic diagenesis. Geochem. Cosmochim. Acta 43 (7), 1075–1090. https://doi.org/10.1016/0016-7037(79)90095-4.
Gardner, L.R., 2005. A modeling study of the dynamics of porewater seepage from intertidal marsh sediments. Estuar. Coast. Shelf Sci. 62 (4), 691–698. https://doi.org/10.1016/j.ecss.2004.10.005.
Gibbes, B., Robinson, C., Carey, H., Li, L., Lockington, D., Li, H., 2008a. Tidally driven porewater exchange within offshore intertidal sandbanks: Part I. Field measurements. Estuar. Coast Shelf Sci. 79 (1), 121–132. https://doi.org/10.1016/j.ecss.2008.03.021.
Gibbes, B., Robinson, C., Li, L., Lockington, D., Li, H., 2008b. Tidally driven porewater exchange within offshore intertidal sandbanks: Part II. numerical simulations. Estuar. Coast Shelf Sci. 80 (4), 472–482. https://doi.org/10.1016/j.ecss.2008.08.021.
Gittel, A., Mußmann, M., Sass, H., Cypionka, H., Könneke, M., 2008. Identity and abundance of active sulfate-reducing bacteria in deep tidal flat sediments determined by directed cultivation and CARD-FISH analysis. Environ. Microbiol. 10 (10), 2645–2658. https://doi.org/10.1111/j.1462-2920.2008.01686.x.
Griffioen, J., Klein, J., Van Gaans, P.F.M., 2012. Reaction capacity characterisation of shallow sedimentary deposits in geologically different regions of the Netherlands. J. Contam. Hydrol. 127 (1–4), 30–46. https://doi.org/10.1016/j.jconhyd.2011.04.001.
Hacherl, E.L., Kosson, D.S., Young, L.Y., Cowan, R.M., 2001. Measurement of iron (III) bioavailability in pure iron oxide minerals and soils using anthraquinone-2, 6-disulfonate oxidation. Environ. Sci. Technol. 35 (24), 4886–4893. https://doi.org/10.1021/es010830s.
Harmsen, G.W., 1954. Observations on the formation and oxidation of pyrite in the soil. Plant Soil 5 (4), 324–348. https://doi.org/10.1007/BF01354456.
Hartog, N., van Bergen, P.F., de Leeuw, J.W., Griffioen, J., 2004. Reactivity of organic matter in aquifer sediments: geological and geochemical controls. Geochem. Cosmochim. Acta 68 (6), 1281–1292. https://doi.org/10.1016/j.gca.2003.09.004.
Hartog, N., Griffioen, J., van Bergen, P.F., 2005. Depositional and paleohydrogeological controls on the distribution of organic matter and other reactive reductants in aquifer sediments. Chem. Geol. 216 (1–2), 113–131. https://doi.org/10.1016/j.chemgeo.2004.11.006.
Harvey, J.W., Germann, P.F., Odum, W.E., 1987. Geomorphological control of subsurface hydrology in the creekbank zone of tidal marshes. Estuar. Coast. Shelf Sci. 25 (6), 677–691. https://doi.org/10.1016/0272-7714(87)90015-1.
Hughes, C.E., Binning, P., Willgoose, G.R., 1998. Characterisation of the hydrology of an estuarine wetland. J. Hydrol. 211 (1–4), 34–49. https://doi.org/10.1016/S0022-1694(98)00194-2.
Huisman, D., Kiden, P., 1998. A geochemical record of Late Cenozoic sedimentation history in the southern Netherlands. Geol. Mijnb. 76 (4), 277–292. https://doi.org/10.1023/A:1003212721020.
Jambor, J.L., Dutrizac, J.E., 1998. Occurrence and constitution of natural and synthetic ferrihydrite, a widespread iron oxyhydroxide. Chem. Rev. 98 (7), 2549–2586. https://doi.org/10.1021/cr970105t.
Johnston, S.G., Keene, A.F., Bush, R.T., Burton, E.D., Sullivan, L.A., 2009. Remediation of coastal acid sulfate soils by tidal inundation: Effectiveness and geochemical implications. Proceedings of 18th NSW Coastal Conference, Ballina, NSW, 3-6 November, East Coast Conferences. Coffs Harbour, NSW.
Johnston, S.G., Keene, A.F., Bush, R.T., Burton, E.D., Sullivan, L.A., Isaacson, L., McElnea, A.E., Ahern, C.R., Smith, C.D., Powell, B., 2011. Iron geochemical zonation in a tidally inundated acid sulfate soil wetland. Chem. Geol. 280 (3–4), 257–270. https://doi.org/10.1016/j.chemgeo.2010.11.014.
Jun, S.-C., Bae, G.-O., Lee, K.-K., 2013. Factors causing dynamic variations in the saltwater–freshwater transition zone in a beach aquifer, Mangsang, South Korea. Hydrogeol. J. 21 (6), 1355–1371. https://doi.org/10.1007/s10040-013-0995-y.
Kaczorek, D., Sommer, M., 2003. Micromorphology, chemistry, and mineralogy of bog iron ores from Poland. Catena 54 (3), 393–402. https://doi.org/10.1016/S0341-8162(03)00133-4.
Royal Netherlands Meteorological Institute (KNMI) a. Regional differences in the extreme rainfall climatology in the Netherlands. Retrieve from https://www.knmi.nl/kennis-en-datacentrum/achtergrond/regional-differences-in-the-extreme-rainfall-climatology-in-the-netherlands. Accessed July 2016.
Royal Netherlands Meteorological Institute (KNMI) b. Verdamping in Nederland. https://www.knmi.nl/kennis-en-datacentrum/achtergrond/verdamping-in-nederland. Accessed July 2016.
Koch, M.S., Maltby, E., Oliver, G.A., Bakker, S.A., 1992. Factors controlling denitrification rates of tidal mudflats and fringing salt marshes in south-west England. Estuar. Coast. Shelf Sci. 34 (5), 471–485. https://doi.org/10.1016/S0272-7714(05)80118-0.
Kolditz, K., Dellwig, O., Barkowski, J., Beck, M., Freund, H., Brumsack, H.-J., 2009. Effects of de-embankment on porewater geochemistry of salt marsh sediments. J. Coast Res. 25 (6), 1222–1235. https://doi.org/10.2112/08-1053.1.
Kolditz, K., Dellwig, O., Barkowski, J., Badewien, T.H., Freund, H., Brumsak, H.-J., 2012. Geochemistry of salt marsh sediments deposited during simulated sea-level rise and consequences for recent and Holocene coastal development of NW Germany. Geo Mar. Lett. 32 (1), 49–60. https://doi.org/10.1007/s00367-011-0250-2.
Kooistra, M.J., 1981. The determination of iron, manganese, sulphur and phosphorus in thin sections of recent marine intertidal sediments in the south-west of the Netherlands by SEM-EDXRA. In: Bisdom, E.B.A. (Ed.), Submicroscopy of soils and weathered rocks. PUDOC, Wageningen, pp. 217–236.
Kostka, J.E., Luther, G.W., 1994. Partitioning and speciation of solid phase iron in saltmarsh sediments. Geochem. Cosmochim. Acta 58 (7), 1701–1710. https://doi.org/10.1016/0016-7037(94)90531-2.
Kostka, J.E., Roychoudhury, A., van Cappellen, P., 2002. Rates and controls of anaerobic microbial respiration across spatial and temporal gradients in saltmarsh sediments. Biogeochemistry 60 (1), 49–76. https://doi.org/10.1023/A:1016525216426.
Kowalski, N., Dellwig, O., Beck, M., Grunwald, M., Fischer, S., Piepho, M., Riedel, T., Freund, H., Brumsack, H.-J., Böttcher, M.E., 2009. Trace metal dynamics in the water column and porewaters in a temperate tidal system: response to the fate of algae-derived organic matter. Ocean Dynam. 59 (2), 333–350. https://doi.org/10.1007/s10236-009-0192-7.
Kuroda, P.K., Sandell, E.B., 1954. Geochemistry of molybdenum. Geochem. Cosmochim. Acta 6 (1), 35–63. https://doi.org/10.1016/0016-7037(54)90028-9.
Lemke, A., Lunau, M., Stone, J., Dellwig, O., Simon, M., 2009. Spatio-temporal dynamics of suspended matter properties and bacterial communities in the back-barrier tidal flat system of Spiekeroog Island. Ocean Dynam. 59 (2), 277–290. https://doi.org/10.1007/s10236-009-0190-9.
Lord, C.J., Church, T.M., 1983. The geochemistry of salt marshes: Sedimentary ion diffusion, sulfate reduction, and pyritization. Geochem. Cosmochim. Acta 47 (8), 1381–1391. https://doi.org/10.1016/0016-7037(83)90296-X.
Louters, T., van den Berg, J.H., Mulder, P.M., 1998. Geomorphological changes of the Oosterschelde tidal system during and after the implementation of the Delta project. J. Coast Res. 14 (3), 1134–1151.
Luther, G.W., Giblin, A., Howarth, R.W., Ryans, R.A., 1982. Pyrite and oxidized iron mineral phases formed from pyrite oxidation in salt marsh and estuarine sediments. Geochem. Cosmochim. Acta 46 (12), 2665–2669. https://doi.org/10.1016/0016-7037(82)90385-4.
Ma, Z., Ysebaert, T., van der Wal, D., de Jong, D.J., Li, X., Herman, P.M.J., 2014. Long-therm salt marsh vertical accretion in a tidal bay with reduced sediment supply. Estuar. Coast Shelf Sci. 146, 14–23. https://doi.org/10.1016/j.ecss.2014.05.001.
Mazumdar, A., Peketi, A., Joao, H., Dewangan, P., Borole, D.V., Kocherla, M., 2012. Sulfidization in a shallow coastal depositional setting: Diagenetic and palaeoclimatic implications. Chem. Geol. 322–323, 68–78. https://doi.org/10.1016/j.chemgeo.2012.06.005.
Mehra, O.P., Jackson, M.L., 1958. Iron oxide removal from soils and clays by a dithionite-citrate system buffered with sodium bicarbonate. Clay Clay Miner. 7 (1), 317–327. https://doi.org/10.1346/CCMN.1958.0070122.
Middelburg, J.J., Herman, P.M.J., 2007. Organic matter processing in tidal estuaries. Mar. Chem. 106 (1–2), 127–147. https://doi.org/10.1016/j.marchem.2006.02.007.
Morford, J.L., Martin, W.R., François, R., Carney, C., 2009. A model for uranium, rhenium, and molybdenum diagenesis in marine sediments based on results from coastal locations. Geochem. Cosmochim. Acta 73 (10), 2938–2960. https://doi.org/10.1016/j.gca.2009.02.029.
Oenema, O., 1988. Diagenesis in subrecent marine sediments in the Eastern Scheldt, Southeast Netherlands. J. Sea Res. 22 (3), 253–265. https://doi.org/10.1016/0077-7579(88)90028-2.
Oenema, O., 1989. Distribution and cycling of fine-grained sediment in the Eastern Scheldt, Southeast Netherlands. Geol. Mijnb. 68 (2), 189–200.
Oenema, O., 1990a. Pyrite accumulation in salt marshes in the Eastern Scheldt, southwest Netherlands. Biogeochemistry 9 (1), 75–98. https://doi.org/10.1007/BF00002718.
Oenema, O., 1990b. Sulfate reduction in fine-grained sediments in the Eastern Scheldt, southwest Netherlands. Biogeochemistry 9 (1), 53–74. https://doi.org/10.1007/BF00002717.
Oenema, O., DeLaune, R.D., 1988. Accretion rates in salt marshes in the Eastern Scheldt, South-west Netherlands. Estuar. Coast Shelf Sci. 26 (4), 379–394. https://doi.org/10.1016/0272-7714(88)90019-4.
Pallud, C., van Cappellen, P., 2006. Kinetics of microbial sulfate reduction in estuarine sediments. Geochem. Cosmochim. Acta 70 (5), 1148–1162. https://doi.org/10.1016/j.gca.2005.11.002.
Passos, E.D.A., Alves, J.C., dos Santos, I.S., Alves, J.D.P.H., Garcia, C.A.B., Spinola Costa, A.C., 2010. Assessment of trace metals contamination in estuarine sediments using a sequential extraction technique and principal component analysis. Microchem. J. 96 (1), 50–57. https://doi.org/10.1016/j.microc.2010.01.018.
Postma, H., 1981. Exchange of materials between the North Sea and the Wadden Sea. Mar. Geol. 40 (1–2), 199–215. https://doi.org/10.1016/0025-3227(81)90050-5.
Redelstein, R., Dinter, T., Hertel, D., Leuschner, C., 2018. Effects of inundation, nutrient availability and plant species diversity on fine root mass and morphology across a saltmarsh flooding gradient. Front. Plant Sci. 9, 98. https://doi.org/10.3389/fpls.2018.00098.
Rickard, D., Luther, G.W., 2007. Chemistry of iron sulfides. Chem. Rev. 107 (2), 514–562. https://doi.org/10.1021/cr0503658.
Rimstidt, J.D., Vaughan, D.J., 2003. Pyrite oxidation: A state-of-the-art assessment of the reaction mechanism. Geochem. Cosmochim. Acta 67 (5), 873–880. https://doi.org/10.1016/S0016-7037(02)01165-1.
Ritsema, C.J., Groenenberg, J.E., 1993. Pyrite oxidation, carbonate weathering and gypsum formation in a drained potential acid sulfate soil. Soil Sci. Soc. Am. J. 57 (4), 968–976. https://doi.org/10.2136/sssaj1993.03615995005700040015x.
Robinson, M., Gallagher, D., Reay, W., 1998. Field observations of tidal and seasonal variations in ground water discharge to tidal estuarine surface water. Ground Water Monit. Remediation 18 (1), 83–92. https://doi.org/10.1111/j.1745-6592.1998.tb00605.x.
Robinson, C., Li, L., Barry, D.A., 2007. Effect of tidal forcing on a subterranean estuary. Adv. Water Resour. 30 (4), 851–865. https://doi.org/10.1016/j.advwatres.2006.07.006.
Røy, H., Lee, J.S., Jansen, S., de Beer, D., 2008. Tide-driven deep pore-water flow in intertidal sand flats. Limnol. Oceanogr. 53 (4), 1521–1530. https://doi.org/10.4319/lo.2008.53.4.1521.
Rudnick, R.L., Gao, S., 2003. Composition of the continental crust. In: Rudnick, R.L. (Ed.), The Crust. In: Holland, H.D., Turekian, K.K. (Eds.), Treatise on Geochemistry Elsevier, Amsterdam, pp. 1–64. https://doi.org/10.1016/B0-08-043751-6/03016-4.
Schwertmann, U., Friedl, J., Stanjek, H., 1999. From Fe(III) Ions to ferrihydrite and then to Hematite. J. Colloid Interface Sci. 209 (1), 215–223. https://doi.org/10.1006/jcis.

1998.5899.
Sophocleous, M., 2004. Groundwater Recharge. In: Silveira, L., Wohnlich, S., Usunoff, E.J. (Eds.), Groundwater, in Encyclopedia of Life Support Systems (EOLSS). UNESCO, Eolss, Oxford, UK Accessed from. http://www.eolss.net.
Stoops, G., 1983. SEM and light microscopic observations of minerals in bog-ores of the belgian campine. Geoderma 30 (1–4), 179–186. https://doi.org/10.1016/S0166-2481(08)70293-9.
Stoops, G., Eswaran, H., 1985. Morfological characteristics of wet soils. In: Wetland soils: Characterization, Classification and Utilization. International Rice Research Institute, Manila-Philippines, pp. 177–189.
Suttill, R.J., Turner, P., Vaughan, D.J., 1982. The geochemistry of iron in Recent tidal-flat sediments of the Wash area, England: A mineralogical, Mössbauer, and magnetic study. Geochem. Cosmochim. Acta 46 (2), 205–217. https://doi.org/10.1016/0016-7037(82)90247-2.
Thullner, M., Regnier, P., van Cappellen, P., 2007. Modeling microbially induced carbon degradation in redox-stratified subsurface environments-Concepts and open questions. Geomicrobiol. J. 24 (3–4), 139–155. http://doi.org/10.1080/01490450701459275.
van den Berg, J.H., 1986. Aspects of Sediment and Morphodynamics of Subtidal Deposits of the Oosterschelde (the Netherlands). Rijkswaterstaat Communications, The Hague, pp. 128.
van Gaans, P.F.M., Griffioen, J., Mol, G., Klaver, G.T., 2011. Geochemical reactivity of subsurface sediments as potential buffer to anthropogenic inputs: A strategy for regional characterization in the Netherlands. J. Soils Sediments 11 (2), 336–351. https://doi.org/10.1007/s11368-010-0313-4.
van Maldegem, D.C., de Jong, D.J., 2004. Opwassen of verdrinken: Sedimentaanvoer naar schorren in de Oosterschelde, een zandhongerig gedempt getijdesysteem. RIKZ/AB/2003/826x. RIKZ, Middelburg, pp. 61.
Venice system for the classification of marine waters according to salinity. (1958). Limnol. Oceanogr., 3(3), 346-347. http://doi.org/10.4319/lo.1958.3.3.0346.
Vermooten, S., Griffioen, J., Heerdink, R., Visser, A., 2011. Geochemische karakterisering van de geotop van Zeeland. rapport no. TNO-034-UT-2010–02397. TNO, pp. 138.
Viollier, E., Inglett, P.W., Hunter, K., Roychoudhury, A.N., Van Cappellen, P., 2000. The ferrozine method revisited: Fe(II)/Fe(III) determination in natural waters. Appl. Geochem. 15 (6), 785–790. https://doi.org/10.1016/S0883-2927(99)00097-9.
Vorlicek, T.P., Kahn, M.D., Kasuya, Y., Helz, G.R., 2004. Capture of molybdenum in pyrite-forming sediments: Role of ligand-induced reduction by polysulfides. Geochem. Cosmochim. Acta 68 (3), 547–556. https://doi.org/10.1016/S0016-7037(03)00444-7.
Vos, P.C., van Heeringen, R.M., 1997. Holocene geology and occupation history of the Province of Zeeland (SW Netherlands). In: In: Fischer, M.M. (Ed.), Holocene evolution of Zeeland (SW Netherlands), vol. 59. Mededelingen NITG-TNO, Haarlem, pp. 5–109.
Vos, P.C., Zeiler, F.D., Moree, J.M., 2002. Delta-2003, 5000 jaar terugblik, kaartatlas met toelichting. Landschapsreconstructie van de kustdelta van Zuidwest Nedeland in opdracht van het project GEOMOD van het Rijksintrituut voor Kust en Zee (RIKZ) van het Ministerie van Verkeer e Waterstaat. TNO-Rapport NITG 02-096-B. .
Wang, D., Aller, R., Sañudo-Wilhelmy, S.A., 2011. Redox speciation and early diagenetic behavior of dissolved molybdenum in sulfidic muds. Mar. Chem. 125 (1–4), 101–107. https://doi.org/10.1016/j.marchem.2011.03.002.
Wilson, A.M., Gardner, L.R., 2006. Tidally driven groundwater flow and solute exchange in a marsh: Numerical simulation. Water Resour. Res. 42 (1), 1–9. W01405. https://doi.org/10.1029/2005WR004302.
Xia, Y.Q., Li, H.L., 2012. A combined field and modeling study of groundwater flow in a tidal marsh. Hydrol. Earth Syst. Sci. 16 (3), 741–759. https://doi.org/10.5194/hess-16-741-2012.
Zwolsman, J.J.G., Berger, G.W., van Eck, G.T.M., 1993. Sediment accumulation rates, historical input, postdepositional mobility and retention of major elements and trace metals in salt marsh sediments of the Scheldt estuary, SW Netherlands. Mar. Chem. 44 (1), 73–94.